Astrophysical $S(E)$ factor of the $^{15}N(p,\alpha)^{12}C$ reaction at sub-Coulomb energies via the Trojan horse method

M. La Cognata, S. Romano, C. Spitaleri,* S. Cherubini, V. Crucillà, M. Gulino, L. Lamia, R. G. Pizzone, and A. Tumino
Dipartimento di Metodologie Fisiche e Chimiche per l'Ingegneria-Università di Catania, Catania, Italy and Laboratori Nazionali del Sud-INFN, Catania, Italy

R. Tribble, Changbo Fu, V. Z. Goldberg, A. M. Mukhamedzhanov, D. Schmidt, G. Tabacaru, and L. Trache
Cyclotron Institute, Texas A&M University, College Station, Texas 77843, USA

B. F. Irgaziev
1GIK Institute of Engineering Sciences and Technology, Topi, District Swabi, N. W. F. P., Pakistan
(Received 6 March 2007; revised manuscript received 10 August 2007; published 28 December 2007)

The low-energy bare-nucleus cross section for $^{15}N(p,\alpha)^{12}C$ is extracted by means of the Trojan horse method applied to the $^{2}H(^{15}N,\alpha^{12}C)n$ reaction at $E_{beam} = 60$ MeV. For the first time we applied the modified half-off-energy-shell resonant R-matrix method that takes into account off-energy-shell effects and initial- and final-state interactions. In particular it has been shown that inclusion of Coulomb ^{15}N-d scattering and off-shell effects do not affect the determination of the astrophysical factor. Also the simple plane-wave approximation used in previous analyses is justified. The results extracted via the Trojan horse method are compared to direct data in the same energy region and show very good agreement in the energy interval 70–312 keV. These results confirm the extrapolations of the S factor reported in literature.

DOI: 10.1103/PhysRevC.76.065804 PACS number(s): 24.10.−i, 26.20.+f, 25.40.Hs, 27.20.+n

I. INTRODUCTION

An open question in nuclear astrophysics is ^{19}F abundance in the Milky Way [1]. Even its production sites are still a largely debated topic: it has been shown that this isotope is synthesized in type II supernovae explosions as well as in Wolf-Rayet stars and during the AGB phase of stellar evolution [1]. In particular it was shown that it is not possible to explain the observed abundances of ^{19}F in Milky Way giants without taking into account its production in the AGB phases [2].

Large efforts were then devoted to understand how ^{19}F nucleosynthesis proceeds in AGB's and its production chain is extensively discussed in Ref. [3], because the fluorine abundances observed in giants can constrain AGB star models [2]. In this context it has been shown that a key isotope for ^{19}F production in AGB stars is ^{15}N and a crucial role is played by the $^{15}N(p,\alpha)^{12}C$ reaction, removing both proton and ^{15}N nuclei from ^{19}F production chain in the AGB intershell environment. The available reaction rates have at least an 8% uncertainty in the fluorine surface abundance [2], due to a factor 2 difference between NACRE [4] and CF88 [5] reaction rates usually employed in calculations.

For charged-particle-induced reactions, such as $^{15}N(p,\alpha)^{12}C$, the Coulomb barrier, $E_{C.B.}$, (about 2 MeV in the present case), is much higher than the energies of interest ($\leqslant$100 keV), thus implying that the reaction takes place via a tunneling effect with an exponential decrease of the cross section, $\sigma(E) \sim \exp(-2\pi\eta)$ (where η is the Sommerfeld parameter).

The $^{15}N(p,\alpha)^{12}C$ experimental cross section has been measured down to 73 keV [6]. Owing to the strong Coulomb suppression, the behavior of the cross section $\sigma(E)$ at low energy has been extrapolated [4] from higher energies ($E >$ 73 keV) using the astrophysical $S(E)$ factor

$$S(E) = E\sigma(E)\exp(2\pi\eta), \tag{1}$$

where $\exp(2\pi\eta)$ is the inverse of the Gamow factor, which removes the dominant energy dependence of $\sigma(E)$ due to the barrier penetration. Although the $S(E)$ factor allows for an extrapolation with simple energy dependence, large uncertainties to $\sigma(E)$ may be introduced, for instance, because of the presence of unexpected resonances.

A second relevant source of uncertainty in extrapolating the S factor down to zero energy is the enhancement of the S factor due to the electron screening effect. In the extrapolation of the cross section using Eq. (1), it is assumed that the Coulomb potential of the target nucleus and projectile is that resulting from bare nuclei. However, as regards nuclear reactions studied in the laboratory, the target nuclei and the projectiles are usually in the form of neutral atoms or molecules and ions, respectively. Because of the electron clouds surrounding the interacting nuclei, the projectile effectively sees a reduced Coulomb barrier. This, in turn, leads to a higher cross section for screened nuclei, $\sigma_s(E)$, compared to the cross section one would get in the case of bare nuclei $\sigma_b(E)$ [7–9]. Therefore the enhancement factor, defined by the following relation

$$f_{lab}(E) = \sigma_s(E)/\sigma_b(E) \approx \exp(\pi\eta U_e/E), \tag{2}$$

where U_e is the so-called electron screening potential [7–9], must be taken into account to determine the bare nucleus cross section.

*Spitaleri@lns.infn.it

Although it is sometimes possible to measure cross sections in the Gamow energy range (see, for example, the discussion in Ref. [10]), the bare nucleus cross section σ_b is often extracted by extrapolating direct data at higher energies where a negligible electron screening contribution is expected. This method has been adopted, for example, in the ^{3}He$(d, p)^4$He reaction to determine the behavior of the astrophysical S factor below 30 keV ([10] and references therein). Anyway alternative methods for determining bare-nucleus cross sections of astrophysical interest are highly required because of the large uncertainties introduced in the extrapolation procedure. An additional source of uncertainty is related to the present poor understanding of the electron screening effect. Indeed, though the electron screening potential has been experimentally deduced for many reactions ([9,10] and references therein), experimental U_e values were found to be much larger than the upper theoretical estimates, i.e., the adiabatic limits [7–9].

In this context a number of indirect methods, the Coulomb dissociation [11–16], the asymptotic normalization coefficient (ANC) method [17–25], and the Trojan horse method (THM) [26–30] were developed. Some of these make use of direct reaction mechanisms, such as transfer processes (stripping and pick-up) and quasi-free reactions (knock-out reactions). In particular, the THM is a powerful tool that selects the quasi-free (QF) contribution of an appropriate TH reaction performed at energies well above the Coulomb barrier to extract a charged-particle binary reaction cross section at astrophysical energies free of Coulomb suppression. The THM has already been applied several times to reactions connected with fundamental astrophysical problems. A list of the reactions studied via the THM is reported in Table I.

The present work reports on a new recent investigation of the ^{15}N$(p, \alpha)^{12}$C reaction. Preliminary results obtained from a single detector configuration have been reported in previous work [31]. The ^{15}N$(p, \alpha)^{12}$C reaction is studied through the ^{2}H(^{15}N,α^{12}C)n TH reaction and its astrophysical $S(E)$ factor is extracted. The ^{15}N$(p, \alpha)^{12}$C reaction proceeds in the astrophysically relevant energy region through a $J^\pi = 1^-$ state in the intermediate ^{16}O nucleus at $E_x = 12.44$ MeV ($\Gamma = 91$ keV) [32], associated with the resonance at $E_{\text{c.m.}} = 312$ keV in the ^{15}N-p excitation function. To extract the astrophysical factor in our previous publications (see Ref. [31] and references therein) the plane-wave approximation for the initial and final-state scatterings of the nuclei in the TH reaction was used. This approximation led to a factorized form of the TH double differential cross section. In the THM the transferred particle is virtual (off-energy-shell). However, we neglected the off-shell character of the transferred particle and used the on-shell approximation. Here, for the first time, we take into account the off-shell character of the transferred proton by applying a HOES R-matrix analysis and estimate the impact of the Coulomb ^{15}N-d scattering in the entry channel of the TH reaction ^{2}H(^{15}N,α^{12}C)n.

II. THEORY

The reaction

$$A + a \rightarrow C + c + s, \tag{3}$$

which we call the Trojan horse reaction, is used in the THM to determine the energy dependence of the cross section for the binary subreaction

$$A + x \rightarrow C + c. \tag{4}$$

It is assumed here that nucleus a has a strong $x \oplus s$ cluster structure. The TH reaction, which is 2 particles $\rightarrow$ 3 particles process (3), can proceed through various reaction mechanisms. In the application of the THM, we are interested in the process that is characterized as a transfer reaction to the continuum, where the Trojan horse a breaks up into a nucleus x that is transferred and where the nucleus s can be regarded as a spectator to the subreaction (4). This direct reaction mechanism gives the dominating contribution to the cross section in a restricted region of the three-body phase space when the momentum transfer to the spectator s is small, i.e., for QF scattering conditions. Because the energy and momentum of the nucleus x do not obey the usual dispersion relation for a

TABLE I. List of the binary reactions connected with fundamental astrophysical problems studied via the THM. The corresponding TH reaction and the beam energy are also reported. The reference list is given in the last column.

Binary reaction	Indirect reaction	E_{lab} (MeV)	Ref.
^{12}C$(\alpha, \alpha)^{12}$C	^{6}Li(^{12}C,α^{12}C)^{2}H	15,18	[63,68]
^{7}Li$(p, \alpha)^4$He	^{2}H(^{7}Li,$\alpha\alpha$)n	19,19.5,20,21	[48,62–65,70,71]
^{6}Li$(d, \alpha)^4$He	^{6}Li(^{6}Li,$\alpha\alpha$)^{4}He	6	[28,49,50,71]
^{6}Li$(p, \alpha)^3$He	^{6}Li$(d, \alpha\ ^3$He$)n$	14,25	[51,52]
^{9}Be$(p,^6$Li$)^4$He	^{2}H(^{9}Be,$\alpha\ ^6$Li)n	22	[74]
^{10}B$(p,^7$Be$)^4$He	^{2}H(^{10}B,$\alpha\ ^7$Be)n	27	[67]
^{11}B$(p,^8$Be$)^4$He	^{2}H(^{11}B,$\alpha\ ^8$Be)n	27	[47,73]
^{3}He$(d, p)^4$He	^{6}Li(^{3}He,$p\ \alpha)^4$He	5,6	[10,66]
^{2}H$(d, p)^3$H	^{2}H(^{6}Li,$t\ p)^4$He	14	[72]
^{15}N$(p, \alpha)^{12}$C	^{2}H(^{15}N,$\alpha\ ^{12}$C)n	60	[31]
^{1}H$(p, p)^1$H	^{2}H$(p, pp)n$	6	[69]
^{6}Li$(n, t)^4$He	^{2}H(^{6}Li,$n\ \alpha)^1$H	14	[76]
^{7}Li$(p, \alpha)^4$He	^{7}Li(^{3}He,$\alpha\ \alpha)d$	27	[75,77]

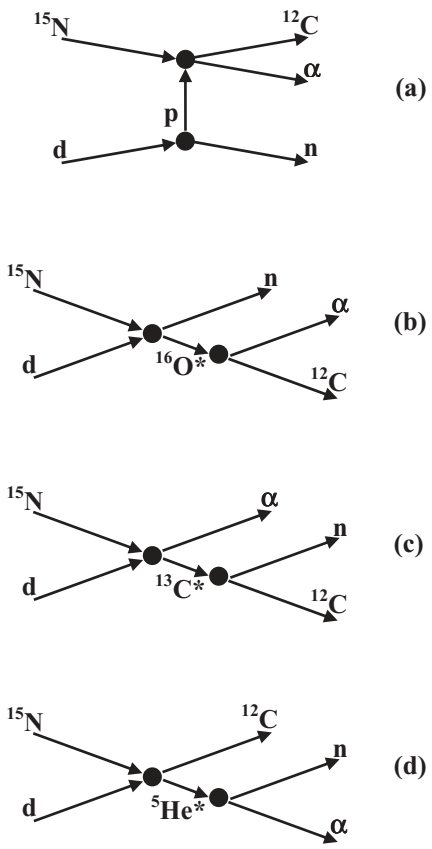

FIG. 1. (a) Diagram representing the quasi-free process ^{2}H(^{15}N,α^{12}C)n; the escaping neutron is considered as spectator to the process, whereas the transferred proton interacts only with the ^{15}N nucleus. (b) Sequential decay mechanism proceeding trough the ^{16}O* compound nucleus, later decaying to the ^{12}C+α channel. (c and d) Two additional examples of sequential decay feeding the ^{12}C+α+n exit channel that can take place in the ^{15}N+d interaction. In (c) the TH reaction proceeds via the formation of the ^{13}C* excited nucleus, subsequently decaying to ^{12}C+n, whereas in (d) the same process involving the ^{5}He$^* \rightarrow {}^4$He+n sequential decay is shown.

free particle, the transferred nucleus appears only as a virtual particle in the reaction process.

A. Quasi-free mechanism and impulse approximation

The QF TH reaction (3) can be described by a Feynman pole diagram shown in Fig. 1(a) ([33] and references therein). In this figure the ^{2}H(^{15}N,α^{12}C)n QF reaction is shown in the pole approximation where the deuteron $a = d$ is the Trojan horse nucleus, the neutron $s = n$ is the spectator and the proton $x = p$ is the transferred virtual particle. The amplitude of the pole diagram describing the TH reaction (3) consists of two factors: the amplitude of the virtual breakup $a \rightarrow s + x$, i.e. $d \rightarrow n + p$ in our case and the amplitude of the binary reaction (4) that is relevant to astrophysics, i.e., ^{15}N$(p, \alpha)^{12}$C in our case.

The QF reaction is well described in the the impulse approximation (IA) formalism [34–45], provided that (i) the momentum in the initial channel is sufficiently high or the associated wavelength is smaller than the nuclear radius of the Trojan horse nucleus a and the incident nucleus A can interact only with the fragment x, leaving the second fragment s as a spectator; (ii) the incident center-of-mass (c.m.) energy is higher than the binding energy of the clusters x and s in a. In the theoretical formalism of the IA, the interaction of the spectator s with the other participating nuclei is neglected and, therefore, the full T matrix describing the reaction mechanism factorizes. Then relations become particularly simple in the plane-wave impulse approximation (PWIA). As desired, the cross section of the TH reaction (3) can be factorized into two terms corresponding to Fig. 1(a) [36–38,40–42,45] by

$$\frac{d^3\sigma}{dE_c d\Omega_c d\Omega_C} \propto [KF\ |\varphi_a(\mathbf{p}_{sx})|^2] \left(\frac{d\sigma}{d\Omega_{\text{c.m.}}}\right)^{\text{HOES}}. \quad (5)$$

KF, which is a kinematical factor containing the final state phase-space factor, is

$$KF = \frac{\mu_{Aa}\, m_c}{(2\pi)^5 \hbar^7} \frac{k_C\, k_c^3}{k_{Aa}} \left[\left(\frac{\mathbf{k}_{Fs}}{\mu_{Fs}} - \frac{\mathbf{k}_{Cc}}{m_c}\right) \cdot \frac{\mathbf{k}_c}{k_c}\right]^{-1}. \quad (6)$$

Here, $\mathbf{k}_j$, m_j, and Ω_j are the momentum, mass, and solid angle of particle j; $\mathbf{k}_{ij}$ and μ_{ij} are the relative momentum and reduced mass of particles i and $j (F = A + x = c + C)$; $\varphi_a(\mathbf{p}_{sx})$ is the Fourier transform of the radial wave function $\varphi_a(\mathbf{r}_{xs})$ for the x-s intercluster relative motion; and $\mathbf{r}_{xs}$ is the x-s relative coordinate. The momentum of the virtual particle x is $\mathbf{p}_x$ and the relative momentum of nucleus i and x is $\mathbf{p}_{ix}$. For the case under consideration, $a = d$, the Hulthén wave function is a good approximation. The factor $[(d\sigma/d\Omega)_{\text{c.m.}}]^{\text{HOES}}$ is the half-off-energy-shell (HOES) differential cross section for the binary reaction (4) at the relative energy E_{xA} of particles x and A in the entry channel given by

$$E_{Ax} = E_{Cc} - Q_{2b}. \quad (7)$$

Here, Q_{2b} is the Q value of the binary reaction (4) and E_{cC} is the relative energy of the outgoing particles C and c.[1]

In the experimental work reported in the present article the validity conditions of the IA appear to be fulfilled. Indeed the sufficiently high ^{15}N beam energy of 60 MeV (1.3 GeV/c in momentum) corresponds to the ^{15}N-d relative momentum k_{aA}^{-1} value of 1.3 fm, which is much smaller than the deuteron effective radius of 4.5 fm. In particular the value of the TH reaction cross section can be determined at $p_{sx} \sim 0$ MeV/c for different combinations of the QF reaction angles and/or different incident energies. In this case the value of the TH reaction cross section divided by the kinematical factor is proportional to the HOES cross section because $\varphi_a(p_{sx} = 0$ MeV/$c)$ is a constant [see Eq. (5)].

To check whether the approximations employed are reliable a number of experiments were carried out to provide critical

[1]We note that for the HOES cross section the relative kinetic energy of the particles A and x in the entry channel of the subreaction and the relative kinetic energy of the exit particles C and c are related by energy conservation (7). The relative momentum of the final particles C and c, which are on-shell, is related to their relative kinetic energy by $k_{Cc} = \sqrt{2\,\mu_{Cc}\, E_{Cc}}$. The relative momentum of the entry particles A and x, due to the off-shell character of x, is related to their relative kinetic energy by a more complicated Eq. (22).

tests of the IA. To this aim, it was suggested [27,28,46,47] that the excitation function and/or the angular distribution of the QF HOES cross section should be measured and compared with the corresponding on-energy-shell (OES) cross section. This leads to two necessary conditions for the factorization of the TH cross section using Eq. (5), namely the agreement between the two data sets in terms of both excitation functions and angular distributions [10,47].

Because $|\varphi_a(\mathbf{p}_{sx})|^2$ is known from nuclear structure studies, the product $[KF\,|\varphi_a(\mathbf{p}_{sx})|^2]$ can be calculated either analytically (for fixed angles) or via a Monte Carlo simulation. Therefore it is possible to determine $(d\sigma/d\Omega_{\mathrm{c.m.}})^{\mathrm{HOES}}$ from a measurement of $d^3\sigma/dE_c d\Omega_c d\Omega_C$ and Eq. (5). The goal of the THM is to determine the astrophysical factor at astrophysically relevant energies. This is achieved by relating the HOES cross section for the binary reaction (4) to the relevant OES astrophysical factor. Normalization of this astrophysical factor to the OES results available from direct measurements at higher energies is a key procedure in the THM allowing one to determine the astrophysical factor down to astrophysically important energies.

B. Half-off-shell *R*-matrix approach

We begin this subsection by explaining why a new theoretical approach for analysis of the resonant binary reactions (4) using the THM is highly desired. In an earlier approach [29,30], called modified plane-wave Born approximation (MPWBA), the HOES binary cross section is replaced by the OES. To explain this, consider the post form of the exact amplitude for the TH reaction

$$\tilde{M}(P,\mathbf{k}_{aA}) = \langle \chi^{(-)}_{\mathbf{k}_{sF}}\,\varphi_s\,\Phi^{(-)}_F|\Delta V_{sF}|\Psi^{(+)}_i\rangle. \tag{8}$$

Here, $\Psi^{(+)}_i$ is the exact $a+A$ scattering wave function; $\Phi^{(-)}_F$ is the wave function of the system $F=C+c=A+x$; $\chi^{(-)}_{\mathbf{k}_{sF}}(\mathbf{r}_{sF})$ is the distorted wave of the system $s+F$; $P=\{\mathbf{k}_{sF},\mathbf{k}_{Cc}\}$ is the six-dimensional momentum describing the three-body system s, C, and c in the final system; $\Delta V_{sF}=V_{sF}-U_{sF}$, $V_{sF}=V_{sC}+V_{sc}=V_{sA}+V_{sx}$ is the interaction potential of s and the system F and U_{sF} is their optical potential. The surface approximation assumes that the TH reaction (3) amplitude has a dominant contribution from the external region where the interaction between the fragments C and c (A and x) can be neglected and the wave function $\Phi^{(-)}_F$ can be replaced by its leading asymptotic form that contains the ingoing wave in the channel $x+A$. The amplitude of this ingoing wave is the OES amplitude for the inverse reaction $C+c\to A+x$. This has been applied earlier for the determination of nonresonant binary reaction cross sections in the THM [48–52]. However, the surface approximation cannot be applied for analysis of the TH reactions proceeding through the resonance in the subsystem $F=A+x\to C+c$ because the dominant contribution comes from the nuclear interior of the subsystem F where both channels $A+x$ and $C+c$ are coupled and where the asymptotic approximation for $\Phi^{(+)}_F$cannot be applied (see Ref. [53]).

The analysis of the TH reaction to determine the resonant binary reaction (4) cross section requires a different approach that takes explicitly into account the off-shell character of the transferred particle x because it is a fundamental feature of the THM. The R-matrix method provides a powerful tool to analyze the resonant reactions. However, the conventional R-matrix approach cannnot be applied for analysis of the TH reactions because of the off-shell character of particle x. In Ref. [53] the theory of the Trojan horse method for resonant binary subreactions has been presented. It is based on the HOES R-matrix approach and takes into account the off-energy-shell effects and initial and final state interactions. We follow the same approach here. We see from Eq. (8) that the wave function $\Phi^{(-)}_F$ contains information about the resonance in the subsystem F. To single out the resonant contribution the wave function $\Phi^{(-)}_F$ in Ref. [53] has been written in the resonant spectral representation given by Eq. (3.8.1) [54]. It is assumed that the resonant reaction $A+x\to C+c$ proceeds through the formation of the intermediate compound state, i.e., the direct coupling between the initial $A+x$ and final $C+c$ channels, which contributes dominantly to direct reactions but gives negligible contribution to resonant ones, is neglected. The resonant spectral decomposition of the wave function $\Phi^{(-)}_F$ is similar to the level decomposition for the wave function in the internal region in the R-matrix approach. Then the TH reaction amplitude in the presence of two interfering resonances in the subsystem F, which is the case under consideration, takes the form (for the sake of simplicity here the spins of the nuclei are neglected) [53]

$$M^{(R)}(P,\mathbf{k}_{aA}) = \sum_{\tau=1,2} \frac{\Gamma^{1/2}_{Cc(\tau)}(E_{Cc})\,M_\tau(\mathbf{k}_{sF},\mathbf{k}_{aA})}{E_{Ax}-E_{R_\tau}+i\,\frac{\Gamma_\tau(E_{Ax})}{2}}, \tag{9}$$

where $\Gamma_{Cc(\tau)}(E_{Cc})$ is the partial observable width of resonance τ in the channel $C+c$, $\Gamma_\tau(E_{Ax})$ is the total observable width of this resonance, and E_{R_τ} its energy. $M_\tau(\mathbf{k}_{sF},\mathbf{k}_{aA})$ is the exact amplitude for the direct transfer reaction $a+A\to s+F_\tau$ populating the compound state F_τ of the system $F=A+x=C+c$:

$$M_\tau(\mathbf{k}_{sF},\mathbf{k}_{aA}) = \langle \chi^{(-)}_{sF}\,\varphi_s\,\Phi_\tau|\Delta V_{sF}|\Psi^{(+)}_i\rangle. \tag{10}$$

Equation (9) is like the two-level, two-channel R-matrix amplitude when the distance between the interfering resonances is significantly larger than the widths of the resonances [55]. The only difference between the OES R-matrix amplitude for the binary resonant reactions $A+x\to C+c$ and the HOES R-matrix amplitude for the TH reaction $a+A\to C+c+s$ is the presence in the latter of the off-shell form factors $M_\tau(\mathbf{k}_{sF},\mathbf{k}_{aA})$ rather than the corresponding partial width amplitudes for the entry channel $A+x$. The amplitude $M_\tau(\mathbf{k}_{sF},\mathbf{k}_{aA})$ may be considered a generalized form factor in the TH resonant amplitude that takes into account the off-energy-shell character of the transferred particle x. Note also that the amplitude $M_\tau(\mathbf{k}_{sF},\mathbf{k}_{aA})$ contains only the penetration factors in the initial channel $a+A$ and final channel $s+F$ of the transfer reaction $a+A\to s+F_\tau$ rather then the penetration factor in the subchannel $A+x$. That is why the TH amplitude is not affected by the Coulomb barrier in the

channel $A + x$. Then the triple TH differential cross section is

$$\frac{d^3\sigma}{dE_c d\Omega_c d\Omega_C} \propto |KF| \left| \sum_{\tau=1,2} \frac{\Gamma^{1/2}_{Cc(\tau)}(E_{Cc})\, M^{\rm DW}_{\tau}(\mathbf{k}_{sF}, \mathbf{k}_{aA})}{E_{Ax} - E_{R_\tau} + i\frac{\Gamma^{1/2}_{\tau}(E_{Ax})}{2}} \right|^2 . \tag{11}$$

The goal of the THM is to determine the energy dependence of the astrophysical factor at the astrophysically relevant energies. It is achieved by normalizing the TH triple differential cross section to the OES experimental astrophysical factor at the resonance peak E_{R_1} (we assume that $E_{R_1} < E_{R_2}$) where the contribution from the second resonance can be neglected. This normalization, which can be done by multiplying the TH triple differential cross section by the factor $(\pi\, e^{2\pi\,\eta_{Ax}})/(2\mu_{Ax})\,\Gamma_{Ax(1)}(E_{Ax})\,|KF|^{-1}\,|M^{\rm DW}_{\tau}(\mathbf{k}_{sF}, \mathbf{k}_{aA})|^{-2}$, provides the astrophysical factor determined from the TH reaction [53]:

$$S^{\rm TH}(E_{xA}) = \frac{\pi\, e^{2\pi\,\eta_{Ax}}}{2\mu_{Ax}}\,\Gamma_{Ax(1)}(E_{Ax}) \times \left| \left[\frac{\Gamma^{1/2}_{Cc(1)}(E_{Cc})}{E_{Ax} - E_{R_1} + i\,\frac{\Gamma_1(E_{Ax})}{2}} + \frac{\Gamma^{1/2}_{Cc(2)}(E_{Cc})\, M_{21}}{E_{Ax} - E_{R_2} + i\,\frac{\Gamma_\tau(E_{Ax})}{2}} \right] \right|^2 . \tag{12}$$

Here, $M_{21} = M_2(\mathbf{k}_{yF}, \mathbf{k}_{aA})/M_1(\mathbf{k}_{yF}, \mathbf{k}_{aA})$ is the ratio of the exact transfer reaction amplitudes to the resonant states F_2 and F_1, which is practically constant in the interval of a few hundreds keV $E_{Ax} \leqslant E_{R_1}$. As we see the normalization of the TH cross section to the available data at the first resonance peak plays a very crucial role in the THM. The energy dependence of the TH astrophysical factor is determined by the ratio M_{21} rather then by the individual transfer reaction amplitudes $M_\tau(\mathbf{k}_{yF}, \mathbf{k}_{aA})$, $\tau = 1, 2$. This ratio is practically constant. It is well known that the direct transfer reaction amplitude is very well approximated by the DWBA amplitude. Hence the ratio M_{21} can be approximated by $M_{21} \approx M^{\rm DW}_2(\mathbf{k}_{yF}, \mathbf{k}_{aA})/M^{\rm DW}_1(\mathbf{k}_{yF}, \mathbf{k}_{aA})$, where

$$M^{\rm DW}_{\tau}(\mathbf{k}_{sF}, \mathbf{k}_{aA}) = \langle \chi^{(-)}_{sF}\, \varphi_s\, \Phi_\tau | \Delta V_{sF} | \varphi_a\, \varphi_A\, \chi^{(+)}_i \rangle \tag{13}$$

is the DWBA amplitude of the direct transfer reaction $a + A \to s + F_\tau$ populating the resonance state F_τ described by the wave function Φ_τ. Thus the problem of taking into account the initial- and final-state interactions in the TH reaction is reduced to a calculation of the ratio $M^{\rm DW}_{21}$. But now we can simplify $M^{\rm DW}_{21}$ even more. It is also very well known that a simple plane-wave approximation gives similar angular and energy dependence as DWBA but fails to reproduce the absolute value. Hence a simple plane-wave approximation should work very well when calculating the ratio M_{21}. This explains why a simple plane-wave approximation worked so well in the previous TH analyses [47]. Note that in the plane-wave approximation $M^{\rm DW}_{\tau}(\mathbf{k}_{sF}, \mathbf{k}_{aA})$ is replaced by

$$M^{0}_{\tau}(\mathbf{k}_{sF}, \mathbf{k}_{aA}) = \langle e^{i\mathbf{k}_{sF}\cdot\mathbf{r}_{sF}}\, \varphi_s\, \Phi_\tau | V_{sA} + V_{xA} | \varphi_a\, \varphi_A\, e^{i\,\mathbf{k}_{aA}\cdot\mathbf{r}_{aA}} \rangle . \tag{14}$$

The post and prior forms are equivalent but the post form is more convenient for our purpose. For sufficiently high momentum of the the projectile A in the QF kinematics, it will interact dominantly with the fragment x while the contribution of the term with V_{sA} is minimized. Consequently, we neglect the term containing V_{sA} below. Then the transfer reaction amplitude in the plane-wave approximation takes the form

$$M^{0}_{\tau}(\mathbf{k}_{sF}, \mathbf{k}_{aA}) \approx \left\langle e^{i\mathbf{k}_{sF}\cdot\mathbf{r}_{sF}}\, I^{F_\tau}_{Ax} \middle| \langle V_{xA}\rangle_{Ax} \middle| I^{a}_{sx}\, e^{i\,\mathbf{k}_{aA}\cdot\mathbf{r}_{aA}} \right\rangle, \tag{15}$$

where $I^{F_\tau}_{Ax} = \langle \varphi_A\, \varphi_x | \Phi_\tau \rangle$ is the overlap function of the wave function of the resonance state F_τ and the bound-state wave functions of A and x, $I^{a}_{sx} = \langle \varphi_s\, \varphi_x | \varphi_a \rangle$ is the overlap function of the bound-state wave functions of nuclei a, x and s, and $\langle V_{xA} \rangle = \langle \varphi_A\, \varphi_x | V_{xA} | \varphi_x\, \varphi_A \rangle$. The plane-wave amplitude $M^{0}_{\tau}(\mathbf{k}_{sF}, \mathbf{k}_{aA})$ can be written in a factorized form

$$M^{0}_{\tau}(\mathbf{k}_{sF}, \mathbf{k}_{aA}) = \left[W^{F_\tau}_{Ax}\left(\mathbf{k}_A - \frac{m_A}{m_F}\,\mathbf{k}_F \right) \right]^* \times I^{a}_{sx}\left(\mathbf{k}_s - \frac{m_s}{m_a}\,\mathbf{k}_a \right) . \tag{16}$$

Here, $I^{a}_{sx}(\mathbf{p}_{sx})$ is the Fourier transform of the overlap function $I^{a}_{sx}(\mathbf{r}_{sx})$ and

$$W^{F_\tau}_{Ax}(\mathbf{k}_{Ax}) = \langle e^{i\mathbf{k}_{Ax}\cdot\mathbf{r}_{Ax}} | \langle V_{xA}\rangle_{Ax}(\mathbf{r}_{Ax}) \big| I^{F_\tau}_{Ax}(\mathbf{r}_{Ax}) \rangle \tag{17}$$

is the vertex form factor for $A + x \to F_\tau$. Then Eq. (11) for the TH triple differential cross section takes the form

$$\frac{d^3\sigma}{dE_c d\Omega_c d\Omega_C} \propto |KF| \left| I^{a}_{sx}\left(\mathbf{k}_s - \frac{m_s}{m_a}\,\mathbf{k}_a \right) \right|^2 \times \left| \sum_{\tau=1,2} \frac{\Gamma^{1/2}_{Cc(\tau)}(E_{Cc}) \left[W^{F_\tau}_{Ax}\left(\mathbf{k}_A - \frac{m_A}{m_F}\,\mathbf{k}_F \right) \right]^*}{E_{Ax} - E_{R_\tau} + i\,\frac{\Gamma_\tau(E_{Ax})}{2}} \right|^2 . \tag{18}$$

Now we can get the HOES cross section for the binary subprocess $A + x \to C + c$ from the triple differential cross section

$$\left(\frac{d\sigma}{d\Omega_{\rm c.m.}} \right)^{\rm HOES} \propto \left[\frac{d^3\sigma}{dE_c d\Omega_c d\Omega_C} \right] \frac{1}{KF\ |I^{a}_{sx}(\mathbf{p}_{sx})|^2}, \tag{19}$$

where $\mathbf{p}_{sx} = \mathbf{k}_s - \frac{m_s}{m_a}\,\mathbf{k}_a$. Equation (19) explains and justifies the procedure used in IA (see subsection II A) to connect the triple and binary TH cross sections. Note that in a strict approach the triple differential cross section is expressed in terms of the overlap function I^{a}_{sx} rather then the two-body bound state wave function φ_a. Note that I^{a}_{sx} and φ_a are related by

$$I^{a}_{sx} = S^{1/2}_{sx}\,\varphi_a, \tag{20}$$

where $S^{1/2}_{sx}$ is the spectroscopic factor. The astrophysical factor obtained by normalization of the triple differential cross section or the HOES cross section for the binary subprocess to the available OES astrophysical factor at the first resonance peak is given by Eq. (12) where, in the plane-wave

approximation, M_{21} is replaced by

$$M_{21}^{0} = \frac{\left[W_{Ax}^{F_\tau}\left(\mathbf{k}_A - \frac{m_A}{m_F}\mathbf{k}_F\right)\right]^*}{\left[W_{Ax}^{F_\tau}\left(\mathbf{k}_A - \frac{m_A}{m_F}\mathbf{k}_F\right)\right]^*}. \quad (21)$$

C. From quasi-free reactions to the Trojan horse method

The THM was first proposed by Baur [26]. It was motivated by the observation of a close resemblence of binary and closely related TH reactions under certain kinematical conditions, see, e.g., Ref. [56]. The basic idea is to extract a binary reaction (4) cross section at low energies from a suitable three-body TH reaction (3) at higher energies under appropriate kinematical conditions. The TH reaction is described as the virtual decay of the Trojan horse nucleus a into the clusters x and s and the subsequent interaction of A with x inside the nuclear region, whereby the nucleus s can be considered a spectator during the reaction. If one chooses the bombarding energy E_A high enough to overcome the Coulomb barrier in the entrance channel of the TH reaction, both Coulomb barrier and electron screening effects are negligible.

In the original article [26] it was proposed that the initial velocity of the projectile A is compensated for by the Fermi motion of particle x to reach the low energies for the binary reaction. In this framework, a momentum of the order of hundreds of MeV/c is needed. However, in the case of a Trojan horse nucleus with a predominant $l = 0$ intercluster motion, such momenta populate the tail of the momentum distribution for particle x, making the separation from eventual background reaction mechanisms like sequential decays feeding the same exit channel [see, e.g., Figs. 1(b)–1(d) for the $^{15}\mathrm{N}(p,\alpha)^{12}\mathrm{C}$ reaction] very critical. Moreover, as already mentioned, the tail of the calculated momentum distribution entering Eq. (5) changes depending on the theoretical approach applied (PWIA or DWIA [47]), therefore a very sophisticated treatment might be required to get the relevant binary reaction cross section. In addition, because short intercluster distances are associated with high relative momenta, distortion of the binary cross section owing to the interaction with s could not be neglected.

To overcome these problems, we introduced a different approach [47,52] based on the idea that the initial projectile velocity is compensated for by the binding energy of particle x inside a. Our approach becomes clear by invoking energy and momentum conservation in the three-ray vertex, $a \to s + x$, and in the four-ray vertex, $A + x \to C + c$, of the pole diagram of Fig. 1(a) yielding

$$E_{Ax} = \frac{p_{Ax}^2}{2\,\mu_{Ax}} - \frac{p_{sx}^2}{2\,\mu_{sx}} - \varepsilon_{sx}, \quad (22)$$

where $\varepsilon_{sx} = m_s + m_x - m_a$. In the QF kinematics $p_{sx} = 0$ and

$$E_{Ax} = \frac{p_{Ax}^2}{2\,\mu_{Ax}} - \varepsilon_{sx}. \quad (23)$$

Because the transferred particle x is virtual, $p_{Ax} \neq k_{Ax} = \sqrt{2\,\mu_{xA}\,E_{Ax}}$, where k_{Ax} is the OES relative $A - x$ momentum. Moreover, Eq. (23) demonstrates that $p_{Ax} > k_{Ax}$ in the THM.

Let us consider the coordinate system in which $k_a = 0$. In QF kinematics

$$\mathbf{k}_{Ax} = \frac{m_x\,\mathbf{k}_A - m_A\,\mathbf{p}_x}{m_x + m_A} = \frac{m_x}{m_x + m_A}\,\mathbf{k}_A, \quad (24)$$

where $\mathbf{k}_A$ is the momemtum of projectile A. Then from Eqs. (23) and (24) we get

$$E_{Ax} = \frac{m_x}{m_x + m_A}\,E_A - \varepsilon_{sx}. \quad (25)$$

This equation explains how the binary reaction can be induced at very low energies E_{Ax} in the THM [52]. Even if the energy of projectile A exceeds the Coulomb barrier in the initial channel, $A + a$, of the TH reaction, it is compensated by the binding energy ε_{sx}. Thus the relative energy of the fragments in the initial channel $A + x$ of the binary reaction (4) can be very low and even negative. In contrast, this condition is difficult or impossible to be satisfied in binary reactions due to the Coulomb barrier. We also conclude from Eq. (25) that the energy E_{Ax} is uniquely determined by the incident beam energy E_A in QF kinematics. Hence, determining the energy dependence of the binary reaction cross section from the TH reaction requires changing the beam energy. From a practical point of view it is more convenient to fix the beam energy and vary the relative momentum p_{sx} in the interval $0 \leqslant p_{sx} \leqslant p_{sx}^{(\max)} < \kappa_{sx}$, where $\kappa_{sx} = \sqrt{2\,\mu_{sx}\,\varepsilon_{sx}}$ is the $a = (s\,x)$ bound-state wave number. In this case the kinematics of the experiment given by Eq. (22) deviates slightly from the QF condition. The role of the cutoff, $\Delta p_{sx} = p_{sx}^{(\max)}$, in the p_{sx} momentum distribution of the Fermi motion for s and x in a is to fix the accessible astrophysical energy region. To show this, consider the laboratory system in which the TH nucleus a is at rest, $k_a = 0$, i.e., $\mathbf{p}_{sx} = -\mathbf{p}_x = \mathbf{k}_s$. Then we derive from Eq. (22)

$$E_{Ax} = \frac{m_x}{m_{xA}}\,E_A - \frac{p_s^2}{2\,\mu_{sF}} + \frac{1}{m_{xA}}\,\mathbf{k}_s \cdot \mathbf{k}_A - \varepsilon_{sx}. \quad (26)$$

Thus the astrophysically relevant energy interval at fixed beam energy E_A can be achieved by varying the absolute value and/or direction of the spectator momentum p_s in the laboratory system.

In principle the THM allows one to determine both the energy dependence and absolute value of the astrophysical factor. However, usually we measure only the energy dependence of the TH cross section and not the absolute value because it is much easier to normalize the TH astrophysical S factor to direct data at higher energies where they are well determined than to make absolute measurements of the triple differential cross section. Our procedure has been discussed in many of our previous publications (see Table I). The THM technique is not an alternative to direct measurement, but it operates as a complementary tool allowing to extract the low-energy behavior. Direct data from literature are necessary both for normalization purpose and to perform the validity test of the method before extracting the THM cross section. The normalization factor can be determined by scaling THM results to direct measurements, which are available at energies above the Coulomb barrier. There are two main questions for the application of the THM: the off-shell effects and the

initial- and final-state interactions. While experimental efforts (see Table I) corroborate the THM approach offering a variety of validity tests of the method only recently has it been shown that close agreement between OES and HOES cross sections (in arbitrary units) in case of nonresonant binary reactions is expected because off-energy-shell distortions to the cross section are comparable or smaller than the uncertainty of experimental data [57]. In this work we address, for the first time, the application of the THM to resonant binary reactions taking into account the off-shell effects; see subsection VI A. The presence of the same resonant behavior in the ^{15}N+p low-energy excitation function indirectly extracted via the THM, with respect to direct data [6,58,59], would constitute a further validity test for the method. However, even if the HOES excitation function for the binary reaction extracted from the TH reaction differs from the OES one, by proper renormalization of the indirect excitation function we can obtain the same energy behavior as direct data.

III. EXPERIMENTAL SETUP

The experiment was performed with a 60-MeV ^{15}N beam, with a spot size on target of a diameter of 1 mm and intensities up to 5 enA, which was provided by the K500 superconducting cyclotron at Texas A&M University. The relative beam energy spread was about 10^{-3}. Self-supported deuterated polyethylene targets (CD_2) of about 150 μg/cm^2 thickness were placed at 90° with respect to the beam direction.

The detection setup consisted of a telescope (A) made up of an ionization chamber and a silicon position sensitive detector (single area, resistive redout) (PSD A) to discriminate carbon nuclei and of two silicon PSDs (B, C) placed on the opposite side with respect to the beam direction. Table II shows the most relevant experimental details concerning all the coincidence detectors. The ionization chamber, closed by two 1.5-μm-thick Mylar foil windows, was filled with 60-mbar butane. To lower detection thresholds for the α particle spectra, no ΔE detectors were put in front of PSDs B and C. Thus particle identification was done from the kinematics of the events. Two kinds of events were triggered by using a time-to-amplitude converter (TAC): A-B and A-C coincidences. The alignment of the three detectors was checked by an optical system.

Angular conditions were selected to maximize the expected quasi-free contribution. Indeed they were chosen to cover momentum values p_s of the undetected neutron ranging from 0 to 150 MeV/c. This assures that the bulk of the quasi-free contribution for the breakup process of interest falls inside the investigated region. This feature is expected for a QF reaction involving deuteron breakup because the momentum distribution for the n-p system has a maximum at $p_s = 0$ MeV/c, the relative motion taking place in an s-wave. The angles corresponding to this condition represent what are known as QF angles. This also allows for a cross-check on the method inside and outside the phase-space regions where the quasi-free contribution is expected. The yield of the ^{2}H(^{15}N,^{13}C)^{4}He binary reaction as recorded in the PSD A 2D position-energy spectrum was monitored to perform a continuous check of the deuteron content of the target.

Energy and position signals of the PSDs were processed by standard electronics together with the TAC signals for each coincidence event and sent to the acquisition system for on-line monitoring and data storage for off-line processing.

TABLE II. Laboratory central angles (θ_0), angular ranges spanned ($\Delta\theta$), solid angles subtended ($\Delta\Omega$), distances from the target (d), thickness (s), and intrinsic angular resolution ($\delta\theta$) for each detector.

Detector	θ_0 (deg)	$\Delta\theta$ (deg)	$\Delta\Omega$ (msr)	d (mm)	s (mm)	$\delta\theta$ (deg)
ΔE-A	−15.3	–	–	164	50	–
PSD-A	−15.3	11.9	8.7	240	0.492	0.2
PSD-B	12.7	13.5	11.2	211	0.984	0.3
PSD-C	32.7	18.0	20.0	158	0.984	0.4

IV. DATA ANALYSIS

A. Detector calibrations and selection of the reaction channel

At the initial stage of the measurement, masks with a number of equally spaced slits were placed in front of each PSD to perform a position calibration. A correspondence between position signal from the PSD and detection angle of the particles was then established by measuring the angle of each slit by means of an optical system.

Energy calibration was performed by means of a ^{228}Th α source and by using the α particles from the ^{2}H(^{15}N,α)^{13}C reaction at 60 MeV, feeding a large number of ^{13}C excited states. Some additional runs were performed using a ^{12}C beam at energies of 30 and 72 MeV to measure the elastic and inelastic scattering on gold and carbon targets. This allowed for a more accurate calibration of the telescope A, optimized for ^{12}C nuclei detection. The total kinetic energy of the detected particles was reconstructed off-line, taking into account the energy loss in the target and in the entrance and exit windows of the ionization chamber.

After detector calibration, the first step of the analysis is the identification of the events corresponding to the ^{2}H(^{15}N,α^{12}C)n TH reaction. This is accomplished first through a selection of the carbon locus in the ΔE-E 2D plot as shown in Fig. 2, where carbon and nitrogen loci are marked. Because isotopic discrimination of ^{12}C from ^{13}C is not possible, C events found in E_A vs. E_B and E_A vs. E_C correlation plots are compared to a Monte Carlo simulation for the ^{2}H(^{15}N,α_0^{12}C)n and ^{2}H(^{15}N,α_1^{12}C)n reaction channels. From the comparison, we can conclude that no additional channels contribute in the experimental kinematical loci.

The Q-value spectrum for these events is given in Fig. 3. Two peaks show up corresponding to the ground state and first excited state of ^{12}C (Q values of 2.74 and −1.70 MeV, respectively). The good agreement between the experimental and the theoretical Q values confirms the identification of the reaction channel as well as the accuracy of the calibration. Same results are deduced from the A-C and the A-B couple.

The ^{15}N$(p,\alpha_1)^{12}$C reaction is of negligible astrophysical interest because its cross section is much lower than the

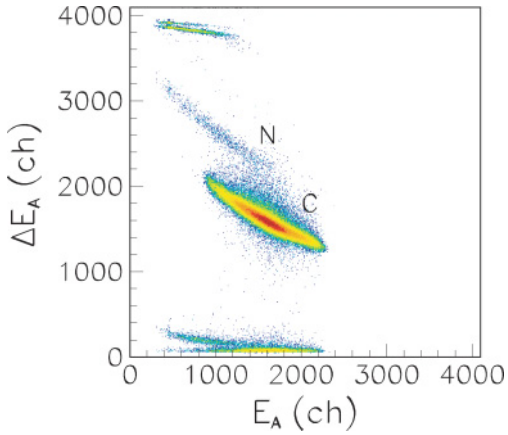

FIG. 2. (Color online) ΔE-E two-dimensional plot for the A telescope. Data are from the A-C coincidence detectors: the A-B couple provides similar results. Carbon locus clearly shows up, ^{12}C and ^{13}C are not resolved because of ionization chamber energy resolution.

^{15}N$(p, \alpha_0)^{12}$C reaction inside the astrophysical relevant energy range [60]. Thus, only events corresponding to the Q-value region $0 \leqslant Q_{3-\text{body}} \leqslant 6$ MeV were considered to extract the ^{15}N$(p, \alpha_0)^{12}$C cross section.

B. Experimental evidence and selection of the quasi-free mechanism

After the selection of the ^{12}C+α_0+n exit channel, the next step in the data analysis was to establish whether the contribution of the QF process to the overall ^{12}C+α coincidence yield is evident in the selected experimental kinematic regions and well separated from other possible reaction mechanisms (see Fig. 1). As already mentioned, because the analysis of the experimental results is complicated by the presence of other reaction mechanisms feeding the same particles in the final state, e.g., sequential decay (SD) and direct breakup (DBU) [10], a thorough study of the processes feeding the exit channel is a necessary step to disentangle the QF component from other mechanisms.

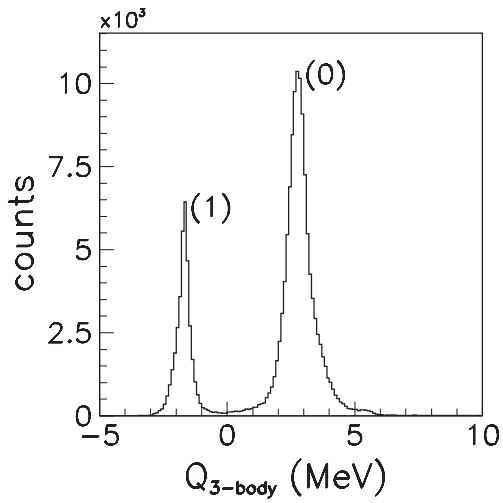

FIG. 3. Q-value plot for the A-C coincidence events. Two dominant peaks corresponding to the ^{2}H(^{15}N,$\alpha_0{}^{12}$C)n ($Q = 2.74$ MeV) and ^{2}H(^{15}N,α_1^{12}C)n ($Q = -1.7$ MeV) reactions are evident (marked with 0, ^{12}C ground state, and 1, ^{12}C first excited state).

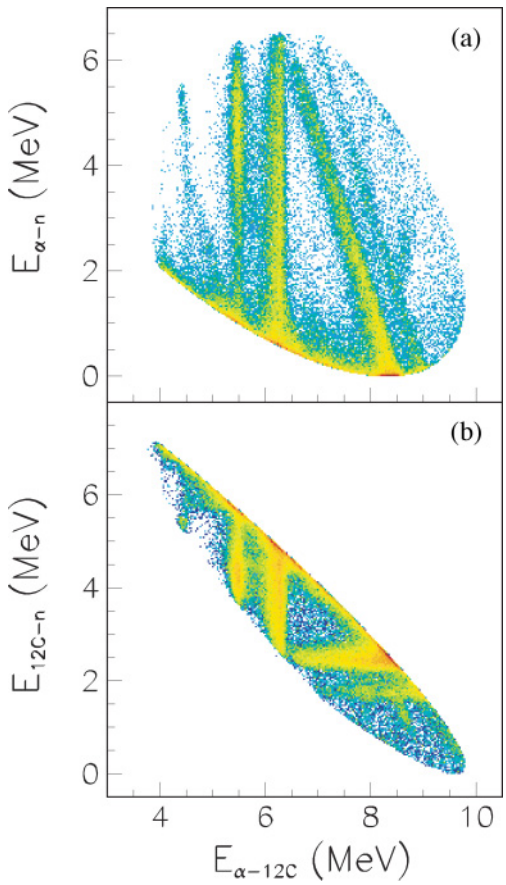

FIG. 4. (Color online) A-C coincidence correlation plots for the relative energies $E_{\alpha n}$ vs. $E_{^{12}\text{C}\alpha}$ (a) and $E_{^{12}\text{C}n}$ vs. $E_{^{12}\text{C}\alpha}$ (b).

To carry out this study, relative energy 2D plots for any two of the three final particles were reconstructed. Relative energies $E_{\alpha n}$ vs. $E_{\alpha\,^{12}\text{C}}$ and $E_{^{12}\text{C}n}$ vs. $E_{\alpha\,^{12}\text{C}}$ are shown in Figs. 4(a) and 4(b), respectively (A-C coincidence). Clear vertical loci appear in both the $E_{\alpha n}$ vs. $E_{\alpha\,^{12}\text{C}}$ and $E_{^{12}\text{C}n}$ vs. $E_{\alpha\,^{12}\text{C}}$ plots (Fig. 4) corresponding to excited states of ^{16}O at 12.44, 13.09, and 13.26 MeV [32]. An additional contribution to the TH cross section due to the sequential decay of ^{13}C excited states at 6.864, 7.492, 7.547, and 7.686 MeV [61] (where the last three levels are not resolved) is also apparent, corresponding to the horizontal loci in Fig. 4(b). Such sequential processes through ^{13}C give a negligible contribution to the coincidence yield at ^{12}C-α relative energies around 5 MeV, which corresponds to the astrophysically relevant energy region in the ^{15}N-p channel [from Eq. (7) one can deduce that zero energy in the ^{15}N$(p, \alpha)^{12}$C channel corresponds to 4.966 MeV in the ^{12}C-α relative energy]. Finally, there is no evidence of levels from ^{5}He sequential decay. Similar results are obtained from A-B coincidences.

The occurrence of sequential mechanisms in the ^{12}C-α channel cannot be ruled out by studying the relative energy correlation plots only, because the same excited states of

the ^{12}C+α system can be formed through a QF reaction mechanism as well as a sequential one [via the channel sketched in Fig. 1(b)]. A way to discriminate between SD and QF events is through the study of the $E_{^{12}C\,\alpha}$ relative energy vs. p_{sx} neutron momentum correlation plot. Indeed the range of the spectator particle momentum spanned in the experiment is such that a comparison of the coincidence yield for small p_{sx} (less than 40 MeV/c) and larger p_{sx} can be performed. A first test allowing to study the reaction mechanisms involved in the population of the ^{16}O states free of phase-space effects is the analysis of angular correlation spectra. This was done to observe the modulation of the TH cross section by the neutron momentum distribution inside the deuteron. Figure 5 shows typical coincidence spectra for the A-C couple projected on the $E_{^{12}C}$ axis and corrected for the phase space effects for a fixed θ_α and for two different $\theta_{^{12}C}$ angles. The coincidence yield is maximum when the neutron momentum approaches zero. The condition of minimum neutron momentum is marked with an arrow in the figures. This feature is expected for a QF reaction because the momentum distribution of the n-p system in the deuteron nucleus has a maximum for $p_{sx} = 0$ MeV/c. The ($\theta_{^{12}C}$, θ_α) angles corresponding to this condition represent what is referred to as QF angles. Similar results have been obtained for other QF angular pairs. This represents a first necessary check for the existence of the QF mechanism in the

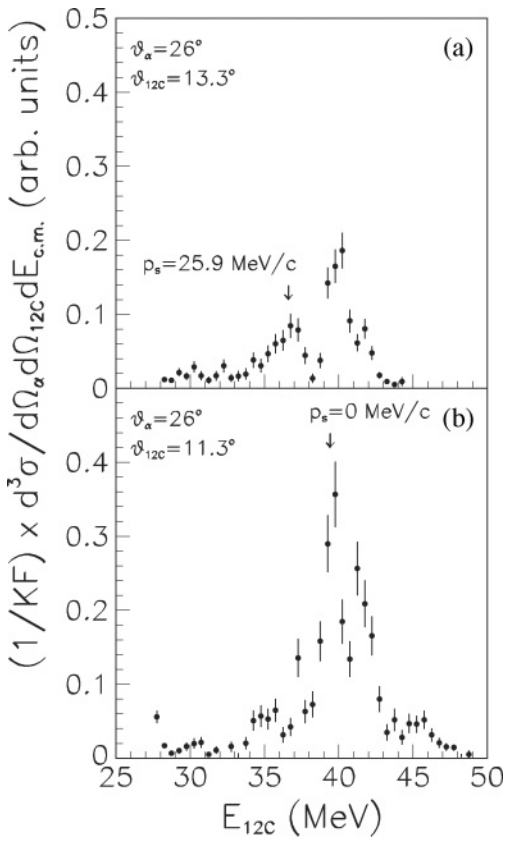

FIG. 5. Typical coincidence spectra for the A-C couple projected on the $E_{^{12}C}$ axis for a fixed θ_α and two different $\theta_{^{12}C}$, within the angular ranges of $\delta_{^{12}C} = \pm 0.6^\circ$ and $\delta_\alpha = \pm 1^\circ$. The condition corresponding to the minimum neutron momentum is marked with an arrow.

^{15}N(p, α)^{12}C reaction. In a similar way $E_{^{12}C}$ spectra for A-B coincidences were obtained for different θ_α while $\theta_{^{12}C}$ was kept fixed. Phase-space effects are removed as in the previous case. The enhancement of the cross section close to zero p_{sx} momentum, which is a necessary condition of the occurrence of the QF mechanism, is also evident.

As a second check to explore the behavior of the coincidence yield for the ^{16}O$^* \rightarrow {}^{12}$C-α channel, the $E_{^{15}Np}$ relative energy spectra were reconstructed for all coincidence events as a function of neutron momentum p_{sx}. The $E_{^{15}N\,p}$ relative energy corresponds to the $E_{\text{c.m.}}$ variable defined in Eq. (7):

$$E_{\text{c.m.}} = E_{^{12}C\,\alpha} - 4.966\ \text{MeV}. \tag{27}$$

These spectra were obtained by selecting different ranges of the neutron momentum p_{sx} and were divided by the phase-space contribution to remove the pure kinematic effects due to the phase-space selection. The ^{12}C-α coincidence yield for $p_{sx} \leqslant 20$ MeV/c [Fig. 6(a)] in detectors A-C appears to be quite high close to the $E_{^{15}N-p}$ resonance energies corresponding to the ^{16}O state at 12.44 MeV. At higher

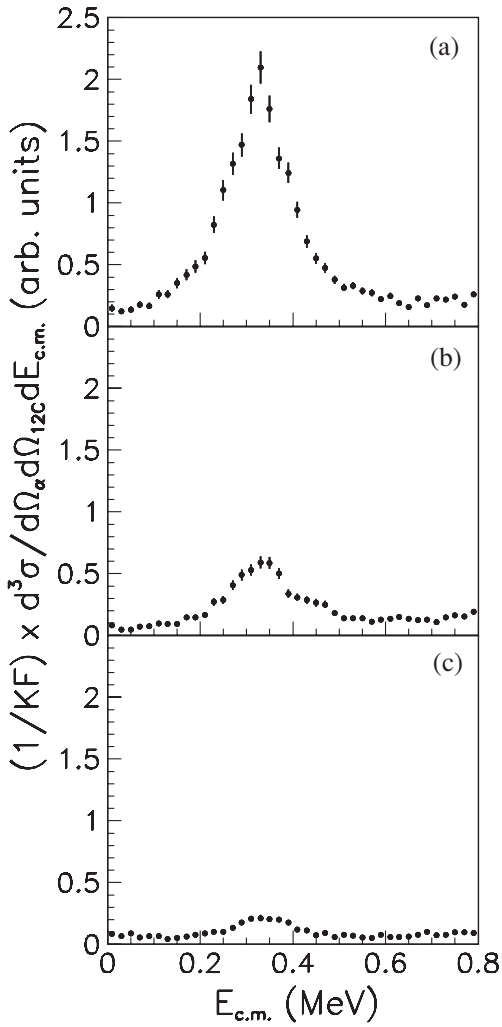

FIG. 6. TH cross section for the A-C coincidences and for different p_{sx} ranges: $p_{sx} < 20$ MeV/c (a), 20 MeV/c $< p_s <$ 40 MeV/c (b) and 40 MeV/c $< p_s <$ 60 MeV/c (c).

momenta $\{20\ \text{MeV}/c \leqslant p_{sx} \leqslant 40\ \text{MeV}/c$ [Fig. 6(b)] and $40\ \text{MeV}/c \leqslant p_{sx} \leqslant 60\ \text{MeV}/c$ [Fig. 6(c)]$\}$, the coincidence yield drastically decreases and becomes barely visible compared to the background. These data provide strong evidence of a clear correlation between coincidence yield and spectator momentum p_{sx}. The same considerations can be drawn for A-B coincidence events.

An observable more sensitive to the reaction mechanism is the shape of the experimental momentum distribution of the undetected neutrons. To reconstruct the experimental p_{sx} distribution, the energy-sharing method [10,47] is applied to each pair of coincidence detectors selecting a narrow $E_{^{15}\text{N}p}$ relative energy window, $\Delta E = 80$ keV for the A-C coincidence and $\Delta E = 200$ keV for the A-B coincidence (because of the lower statistics). Dividing the resulting quasi-free coincidence yield by the kinematic factor, a quantity that is proportional to the product of the p_{sx} momentum distribution and the differential ^{15}N-p binary cross section [see Eq. (5)] is deduced

$$|\varphi_a(\mathbf{p}_{sx})|^2 \left(\frac{d\sigma}{d\Omega_{\text{c.m.}}}\right)^{\text{HOES}}_{E_0} \propto \left[\frac{d^3\sigma}{d\Omega_\alpha d\Omega_{^{12}\text{C}} dE_{\text{c.m.}}}\right][KF]^{-1}, \tag{28}$$

where E_0 is the mean energy of the relative energy window. In a restricted $E_{^{15}\text{N}p}$ relative energy range selected by choosing the energy region between the 12.44-MeV and the 13.09-MeV ^{16}O resonance, the differential binary cross section $(d\sigma/d\Omega_{\text{c.m.}})^{\text{HOES}}$ of the $^{15}\text{N} + p$ reaction can be considered almost constant. Thus the experimental p_{sx} momentum distribution is given in arbitrary units by the equation

$$|\varphi_a(\mathbf{p}_{sx})|^2 \propto \left[\frac{d^3\sigma}{d\Omega_\alpha d\Omega_{^{12}\text{C}} dE_{\text{c.m.}}}\right][KF]^{-1}. \tag{29}$$

The momentum distributions from A-B and A-C coincidences were averaged out after being normalized to each other. This result is compared with the square of a Hulthén wave function in momentum space [47]

$$\varphi_a(\mathbf{p}_{sx}) = \frac{1}{\pi}\sqrt{\frac{ab(a+b)}{(a-b)^2}}\left[\frac{1}{a^2+p_{sx}^2} - \frac{1}{b^2+p_{sx}^2}\right] \tag{30}$$

with parameters $a = 0.2317\ \text{fm}^{-1}$ and $b = 1.202\ \text{fm}^{-1}$ [47] for the deuteron with the normalization constant fixed at the experimental maximum (Fig. 7). The good agreement between the two, together with the previous tests, makes us confident that the QF mechanism gives the main contribution to the ^{15}N+d reaction at an energy of 60 MeV in the selected kinematical experimental regions; the QF mechanism can be selected without significant contribution from contaminant SD processes; the analysis in PWIA is sufficient to describe the process.

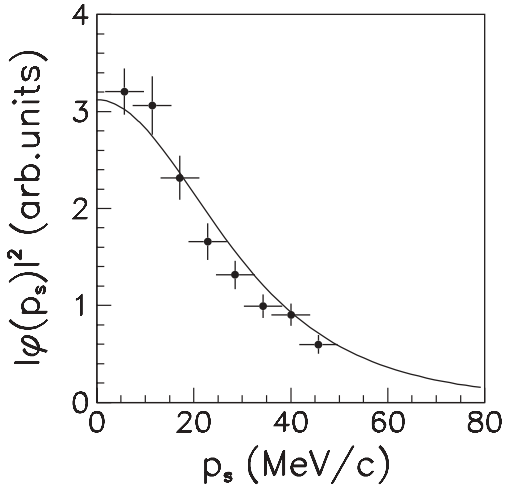

FIG. 7. Average experimental momentum distribution (full dots) obtained from the A-B and A-C ones compared with the theoretical distribution (30) (full line), normalized to the experimental data (see text for details).

V. FROM THE EXPERIMENTAL TROJAN HORSE REACTION TO THE INDIRECT HALF-OFF-ENERGY-SHELL BINARY REACTION CROSS SECTION

A. Angular distributions

As was noted, the THM provides the HOES binary reaction cross section, so it is necessary to perform the appropriate validity tests on the deduced cross section for the adopted IA.

A test involves the comparison between the THM angular distributions and the direct measurements [6]. The emission angle for the ^{12}C nucleus in the α-^{12}C center-of-mass system is calculated according to the relation [37]

$$\theta_{\text{c.m.}} = \arccos\frac{(\mathbf{v}_{^{15}\text{N}} - \mathbf{v}_p)\cdot(\mathbf{v}_\alpha - \mathbf{v}_{^{12}\text{C}})}{|\mathbf{v}_{^{15}\text{N}} - \mathbf{v}_p||\mathbf{v}_\alpha - \mathbf{v}_{^{12}\text{C}}|}, \tag{31}$$

where the vectors $\mathbf{v}_{^{15}\text{N}}, \mathbf{v}_p, \mathbf{v}_\alpha, \mathbf{v}_{^{12}\text{C}}$ are the velocities of projectile, transferred proton, outgoing α-particle, and ^{12}C, respectively. These quantities are calculated from their corresponding momenta in the lab system, where the momentum of the transferred particle is equal and opposite to that of neutron when the quasi-free assumptions are fulfilled [37].

The center-of-mass angular ranges covered in the present experiment were $\theta_{\text{c.m.}} = 80°$–$120°$, $\theta_{\text{c.m.}} = 120°$–$160°$ for the A-C and the A-B detector coincidences, respectively. The angular distribution test was performed for five different energies, within the astrophysically relevant $p - ^{15}$N relative energy range in steps of $\Delta E_{\text{c.m.}} = 100$ keV (± 50 keV energy bin). To select the region where the QF mechanism is dominant, coincidence events for neutron momenta ranging between 0 and 40 MeV/c were considered. A Monte Carlo calculation was then performed to evaluate the $KF|\varphi_a(\mathbf{p}_{sx})|^2$ product. The momentum distribution in the calculation is that given in Eq. (29). The geometrical efficiency of the experimental setup as well as the detection thresholds of the PSD's were taken into account. Following the PWIA prescription, the binary cross section $(d\sigma/d\Omega_{\text{c.m.}})^{\text{off}}$ was derived by dividing the selected

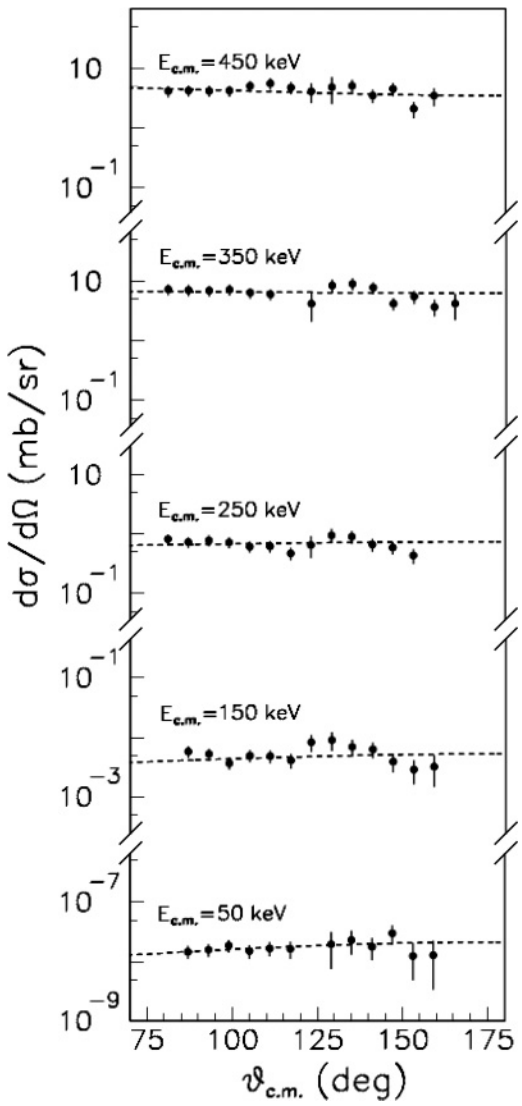

FIG. 8. Indirect angular distributions for the ^{15}N$(p,\alpha)^{12}$C reaction (full dots) for different $E_{^{15}Np}$ relative energies compared to the direct ones from [6] (dashed lines); $E_{Ax} \equiv E$.

three-body coincidence yield by the result of the Monte Carlo calculation.

The results are given in Fig. 8, where the different relative energies are marked for each distribution. The error bars represent both statistical and normalization errors. Normalization is performed over the whole angular region. In Fig. 8, for each $E_{\mathrm{c.m.}}$ energy the angular distributions are compared with the direct cross section extracted from [6]. Good agreement between the two trends shows up, providing confidence in the validity of the IA for the present experimental conditions.

B. Excitation functions

As a second validity test, the behavior of the indirect excitation function is examined to check whether the off-energy-shell binary cross section integrated over the full $\theta_{\mathrm{c.m.}}$ range is consistent with direct data [6,58,59]. Because the THM angular distributions appear to be in good agreement

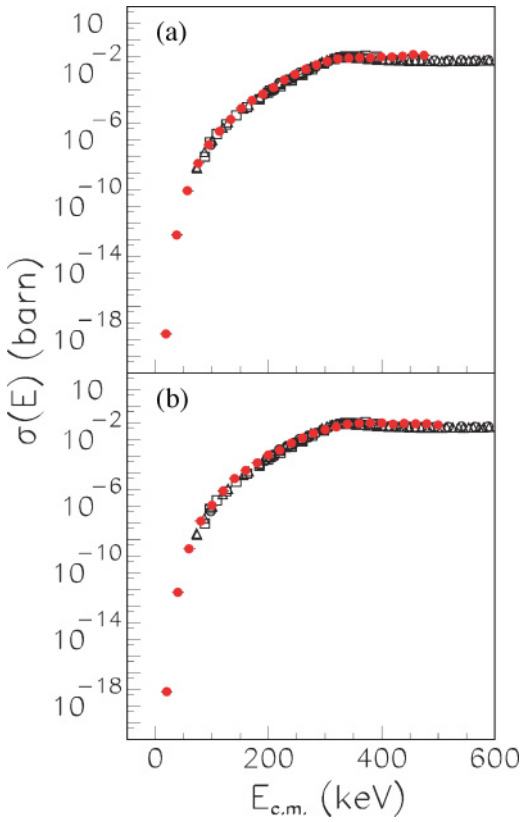

FIG. 9. (Color online) Comparison between the indirect excitation function (full dots) for the ^{15}N$(p,\alpha)^{12}$C reaction and the direct data from Refs. [6,58,59] (open symbols). (a) Reports data from the A-B coincidence detectors, whereas (b) shows the binary cross section from the A-C coincidence.

with the direct ones over the entire energy range explored, their behavior is extrapolated to the $\theta_{\mathrm{c.m.}}$ range not covered in the experiment, assuming the same trend of the direct measurement. Then the indirect binary cross section is integrated over the full $\theta_{\mathrm{c.m.}}$ angular range and multiplied by the Coulomb penetration function as given in Refs. [10,47]. A dominant $l = 0$ partial wave in the entrance channel of the ^{15}N$+p$ binary reaction and a channel radius given by the sum of the radii of the two interacting nuclei have been assumed. This is a necessary step because the investigated ^{15}N$+p$ relative energy region lies below the Coulomb barrier (about 2 MeV) and the extracted THM binary cross section is free of Coulomb suppression as discussed above. Normalization to the direct behavior was performed in the resonant region between $E_{\mathrm{c.m.}} = 200$ and 400 keV. To do this, both direct and THM resonances were fitted by using Breit-Wigner shapes. The normalization factor was fixed by requiring the same area for the two curves.

The final binary cross section obtained in the present work is shown in Fig. 9 (red full dots), where direct data are also given (open symbols). The upper panel in Fig. 9(a) refers to the A-B coincidence detectors while the lower one [Fig. 9(b)] shows the binary cross section extracted from A-C coincidence events. The good agreement between the data sets is a necessary condition for the further extraction of the astrophysical $S(E)$ factor by means of the THM [10,47,50,52,62,63].

VI. RESULTS AND DISCUSSION

We derive the $S(E)$ factor from our data using the definition in Eq. (1). Moreover, starting from the experimental uncertainties affecting energy and angle of emission of each ejectile, an error estimate for the relative energies $E_{^{15}\mathrm{N}p}$ (the $E_{\mathrm{c.m.}}$ variable) was performed leading to a value of about 10 keV for the A-B coincidences and 40 keV for the A-C coincidences. An overall energy resolution of 1% and angular resolutions of 0.3° for PSD A and PSD B and 0.4° (PSD C) were considered. These numbers account for both angular and energy straggling in the target and in the dead layers. The difference between the two cited energy uncertainties mainly comes from the different experimental conditions, detector C being closer to the target than detector B. In addition, the magnifying glass effect [12] is less relevant for the A-C coincidence, because of the different kinematics. Vertical error bars include both statistical errors and a systematic error coming from the normalization procedure. The S factor extracted from A-C coincidences has a much lower uncertainty due to better statistics than the one derived from A-B coincidences. It also has an 9% normalization error, which is much lower than the 25% normalization error for the S factor for the A-B coincidences.

Because finite resolution affects the two S factors extracted from the A-B and the A-C coincidences in different ways, to combine the two data sets this effects were removed by extracting a curve that best represents the "infinite" energy resolution S factor for our data. The two $S_{\mathrm{bare}}(E)$ data sets obtained through this procedure were then averaged out and the result is shown in Fig. 10 and summarized in Table III. An additional systematic error of ∼16% arising from the deconvolution procedure was added to the data set in Table III and included in the determination of $S(0)$. Direct data from Refs. [6,58,59] are shown as open symbols in Fig. 10. Good agreement is found in the energy range explored by direct data.

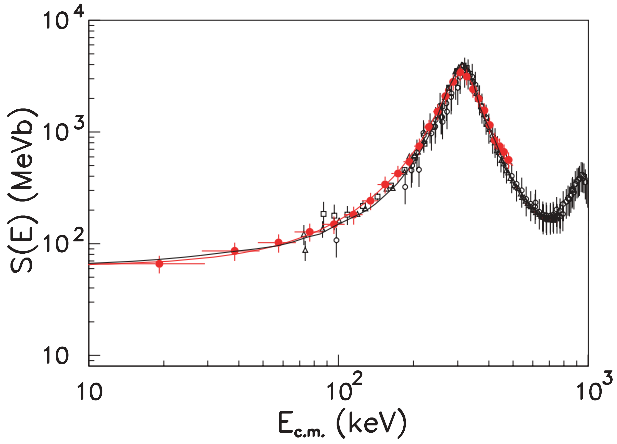

FIG. 10. (Color online) Indirect astrophysical $S(E)$ factor (full red dots) with $E_{Ax} \equiv E$. The data are obtained by averaging the two "infinite" resolution data sets from A-B and A-C coincidences as discussed in the text. The direct data from Refs. [6,58,59] are also shown as open symbols (circles, squares, and triangles, respectively). The red line represents a fit to the THM data by means of the curve of Eq. (32) (the fitting parameters are given in Table IV). For comparison [6] a Breit-Wigner parametrization is also displayed as the black line.

TABLE III. Astrophysical S factor for the $^{15}\mathrm{N}(p,\alpha)^{12}\mathrm{C}$ reaction, from the average of the two "infinite" resolution A-B and A-C S factors. Energy, $S(E)$ factor and corresponding error are reported. See text for detailed discussion.

$E_{\mathrm{c.m.}}$ (MeV)	$S(E)$ (MeV b)	$\Delta S(E)$ (MeV b)
19.2	66	12
38.4	86	16
57.6	102	19
76.8	127	23
96.0	149	27
115.2	181	33
134.4	242	43
153.6	339	59
172.8	425	73
192.0	541	92
211.2	745	125
230.4	1102	182
249.6	1520	249
268.8	2103	342
288.0	2814	456
307.2	3430	558
326.4	3124	504
345.6	2416	392
364.8	1982	323
384.0	1556	255
403.2	1151	191
422.4	841	142
441.6	747	127
460.8	659	113
480.0	561	96
499.2	511	88
518.4	504	86
537.6	462	80
556.8	462	79
576.0	439	75

A fit to the data was performed to extrapolate the S factor to zero relative energy. The functional form used in the fit is given by the sum of a second-order polynomial and a Breit-Wigner function

$$S(E) = a_0 + a_1 E + a_2 E^2 + \frac{W}{(E\text{-}E_R)^2 + \frac{\Gamma^2}{4}} \qquad (32)$$

with parameters a_i $(i = 0, 1, 2)$, W, resonance energy E_R and width Γ; $E \equiv E_{^{15}\mathrm{N}p}$. The best fit parameters are reported in Table IV. The curve well reproduces the indirect THM astrophysical S factor as shown by the χ^2 (Table IV) and displayed in Fig. 10 as a full red line. For comparison, the Breit-Wigner parametrization from Ref. [6] is also shown in Fig. 10, demonstrating the good agreement between the two curves within the experimental uncertainties. The zero-energy S factor for the averaged A-B and A-C coincidences, resulting from the fit, is in good agreement with previous $S(0)$ estimates from direct data measured by Refs. [6,58,59], given in Table V: $S_{\mathrm{bare}}(0) = 62 \pm 10$ MeV b. The quoted uncertainty accounts for statistical, normalization, and extrapolation errors. In addition the $S(E)$ factor obtained here is consistent with the result of the preliminary analysis in Ref. [31] to 20 keV. The lowest energy point, which is affected by the largest

TABLE IV. Fitting parameters for $S(E)$, Eq. (32). The centroid of the Breit-Wigner is fixed at the 1^- resonance energy of 312 keV. In the last column the χ^2 per degree of freedom is also reported.

a_0 (MeV b)	a_1 (MeV b/MeV)	a_2 (MeV b/MeV^2)	Γ (MeV)	W (MeV^{3}b)	χ^2/N
-55 ± 10	-459 ± 140	1928 ± 260	0.118 ± 0.005	11.7 ± 0.3	0.1

uncertainty, both theoretical and experimental, is neglected in the present work.

A. Application of the modified HOES R-matrix approach

In this section we describe the analysis of the astrophysical factor applying the HOES R-matrix approach developed in Ref. [53] and described in subsection II B. Generally speaking the reaction under consideration has contributions from the first three resonances in the $^{15}\mathrm{N} + p$ system at $E_{^{15}\mathrm{N}\,p} =$ 0.312, 0.9624, and 1.0014 MeV, and the subthreshold state at $E_{^{15}\mathrm{N}\,p} = -2.53$ MeV. In the HOES R-matrix method approach, the resonance width in the entry channel, which appears in the standard R-matrix, is replaced by the form factor that is the amplitude of the direct transfer reaction $d + {}^{15}\mathrm{N} \rightarrow n + {}^{16}\mathrm{O}_\tau$, $\tau = 1, 2, 3$ populating the resonance state of ^{16}O. These form factors were calculated using the plane-wave approximation, but they were checked by taking into account the Coulomb interaction in the initial state of the direct transfer reaction.

The first two resonances, $E_{^{15}\mathrm{N}\,p} = 0.312$ and 0.9624 MeV and the subthreshold state have the same quantum numbers, $l = 0$, and spin-parity $J^\pi = 1^-$. Hence the amplitudes of the reactions proceeding through these states interfere. The sign of the interference is determined by fitting to the S factor extracted from the THM. In direct measurements the contribution from the resonance at $E_{^{15}\mathrm{N}\,p} = 1.0014$ MeV is suppressed at $E_{^{15}\mathrm{N}\,p} < 500$ keV due to the high centrifugal barrier from to the $l = 2$ orbital momentum of this resonance. In the THM the centrifugal barrier is absent and, consequently, the contribution of this resonance may not be negligible, but both the experimental data and theoretical analysis show that it is negligible.

The THM allows us to investigate the impact of the subthreshold state on the astrophysical factor at low energies, $E_{^{15}\mathrm{N}\,p} < 70$ keV, which are not available to direct measurements. The $^{15}\mathrm{N} + p \rightarrow {}^{12}\mathrm{C} + \alpha$ reaction can proceed through the subthreshold state $E_{^{15}\mathrm{N}\,p} = -2.54$ MeV as follows: the proton is captured to the intermediate bound state of ^{16}O, which is 2.54 MeV below the $^{15}\mathrm{N} + p$ threshold but 2.42 MeV above the threshold of the $^{12}\mathrm{C} + \alpha$ channel. However, we find that the inclusion of the subthreshold state does not affect the both OES and HOES astrophysical factors at low energies and its effect can be neglected. Thus in what follows we consider only the first two 1^- resonances $E_{^{15}\mathrm{N}\,p} = 0.312$ and 0.9624 MeV. Then the HOES astrophysical factor normalized at the first resonance peak to the OES S factor obtained from direct measurements [6] is given by Eq. (12). We rewrite this equation here, showing explicitly all the kinematical factors including the spins of the nuclei, as

$$S^{\mathrm{TH}}(E_{Ax}) = \pi\,\lambda_N^2\,\frac{1}{2}\,\frac{(2\,J+1)}{(2\,J_x+1)(2\,J_A+1)}\,\frac{1}{\mu_{Ax}}\,e^{2\,\pi\,\eta_{Ax}}\,10^{-2} \times \Gamma_{Ax(1)}(E_{Ax}) \left| \frac{\sqrt{\Gamma_{Cc(1)}\,(E_{Cc})}}{E_{Ax} - E_{Ax(R1)} + i\,\frac{\Gamma_{(1)}}{2}} + \frac{\sqrt{\Gamma_{Cc(2)}\,(E_{Cc})}\,M_{21}^0}{E_{Ax} - E_{Ax(R2)} + i\,\frac{\Gamma_{(2)}}{2}} \right|^2 . \tag{33}$$

Here, $\lambda_N = 0.2118$ fm is the nucleon Compton wave length, J is the resonance spin, J_i is the spin of nucleus i, and μ_{Ax} is the reduced mass of A and x expressed in atomic mass units. If energies and resonance widths are expressed in MeV, the TH astrophysical factor $S^{\mathrm{TH}}(E_{Ax})$ is given in MeV b. In the case under consideration, $x = p$, $A = {}^{15}\mathrm{N}$, $c = \alpha$, $C = {}^{12}\mathrm{C}$. In the plane-wave approximation, the ratio $M_{21} = M_{21}^0$ is given by Eq. (21).

The TH HOES astrophysical factor is to be compared with the OES one

$$S(E_{Ax}) = \pi\,\lambda_N^2\,\frac{1}{2}\,\frac{(2\,J+1)}{(2\,J_x+1)(2\,J_A+1)}\,\frac{m_x+m_A}{m_x\,m_A}\,e^{2\,\pi\,\eta_{Ax}}\,10^{-2} \times \Gamma_{Ax(1)}(E_{Ax}) \left| \frac{\sqrt{\Gamma_{Cc(1)}\,(E_{Cc})}}{E_{Ax} - E_{Ax(R1)} + i\,\frac{\Gamma_{(1)}}{2}} + \frac{\sqrt{\Gamma_{Cc(2)}\,(E_{Cc})}\,\gamma_{Ax(21)}}{E_{Ax} - E_{Ax(R2)} + i\,\frac{\Gamma_{(2)}}{2}} \right|^2 . \tag{34}$$

Here

$$\gamma_{Ax(21)} = \sqrt{\frac{\Gamma_{Ax(2)}\,(E_{Ax})}{\Gamma_{Ax(1)}\,(E_{Ax})}} = \frac{\gamma_{Ax(2)}}{\gamma_{Ax(1)}} \tag{35}$$

is the ratio of the reduced widths of the levels 2 and 1. In Eq. (35) we took into account that $\Gamma_{Ax(i)}(E) = 2\,P_{l_i}(k_{Ax}\,r_0)\,\gamma_{Ax(i)}^2$, where $P_{l_i}(k_{Ax}\,r_0)$ is the penetrability factor for the system $A + x$ with relative orbital angular momentum

TABLE V. Astrophysical $S(0)$ factors (and the corresponding errors) for the $^{15}\mathrm{N}(p,\alpha)^{12}\mathrm{C}$ reaction extrapolated by different authors [6,58,59], compared with the ones deduced in the present work: (1) polynomial fit and [(2), (3), and (4)] modified R-matrix calculation (4.5-, 5.0-, and 5.5-fm channel radius, respectively).

$S(0)$ (MeV b)	$\Delta S(0)$ (MeV b)	Ref.
64	–	[58]
78	6	[59]
65	4	[6]
62	10	(1)
63	10	(2)
65	10	(3)
68	11	(4)

l_i, r_0 is the channel radius, $k_{Ax} = \sqrt{2\,\mu_{Ax}\,E_{Ax}}$. Hence $\gamma_{Ax(21)}$ is the ratio of the reduced widths and does not depend on energy. To find M^0_{21} we used Eq. (17) in which we approximated the overlap function $I^{F_{(i)}}_{Ax}$ by a single-particle ^{15}N-p wave function in the Woods-Saxon potential calculated in the internal region by a procedure similar to that used in the R-matrix method to calculate the level eigenfunctions. For the resonances at $E_x = 13.09$ MeV and $E_x = 12.44$ MeV in ^{16}O, the experimental ratio $\gamma_{Ax(21)} = 1.1 \pm 0.1$ MeV, while the calculated $M^0_{21} \approx 1.13$ in the energy interval $E_{Ax} \leqslant 312$ keV. The coincidence of M^0_{21} and $\gamma_{Ax(21)}$ explains why the HOES astrophysical factor $S^{\rm TH}(E_{Ax})$ extracted from the TH reaction agrees with the OES astrophysical factor at low energies.

The results of the calculation of $S^{\rm TH}(E_{Ax})$ are shown in Fig. 11, where they are compared with THM data. When calculating $S^{\rm TH}(E_{Ax})$ we assumed destructive interference between the 12.44 MeV and the 13.09 MeV $J^\pi = 1^-$ ^{16}O resonances at energies $E_{Ax} < 312$ keV. The same interference occurs between these resonances when fitting the direct measurements. According to Eq. (33) we need to know, in addition to M^0_{21}, the proton and α partial widths and energies of the first two 1^- resonances to calculate the astrophysical factor $S^{\rm TH}(E_{Ax})$. These parameters have been determined by fitting direct measurements [6,58,59]. The best fit has been achieved for $E_{R_1} = 312$ keV, $\Gamma_{Ax(1)} \equiv \Gamma_{p(1)} = 1.1$ keV, $\Gamma_{Cc(1)} \equiv \Gamma_{\alpha(1)} = 93.4$ keV, $E_{R_2} = 962.4$ keV, $\Gamma_{Ax(2)} \equiv \Gamma_{p(2)} = 95.31$ keV, and $\Gamma_{Cc(2)} \equiv \Gamma_{\alpha(2)} = 45$ keV. In Fig. 11 three calculations are given for the channel radius: $r_0 = 4.5$ fm (black line), $r_0 = 5.0$ fm (blue line), and $r_0 = 5.5$ fm (red line). The shape of the deduced resonant astrophysical S factor is in very good agreement with the direct data as well as the THM data (e.g., in the case of the $r_0 = 5.0$ fm calculation, a $\chi^2 = 1.9$ per degree of freedom is retrieved). The calculated values of the astrophysical factor $S(0)$ are 63.0 MeV b for $r_0 = 4.5$ fm, 65.0 MeV b for $r_0 = 5.0$ fm, and 68.0 MeV b for $r_0 = 5.5$ fm, agree with the result of direct data extrapolation (see for comparison Table V). Thus we have shown using the HOES R matrix and confirmed by calculations that the THM is a reliable way to determine the resonant astrophysical factor down to zero energy for the binary reaction $^{15}\mathrm{N} + p \rightarrow {}^{12}\mathrm{C} + \alpha$ between bare nuclei.

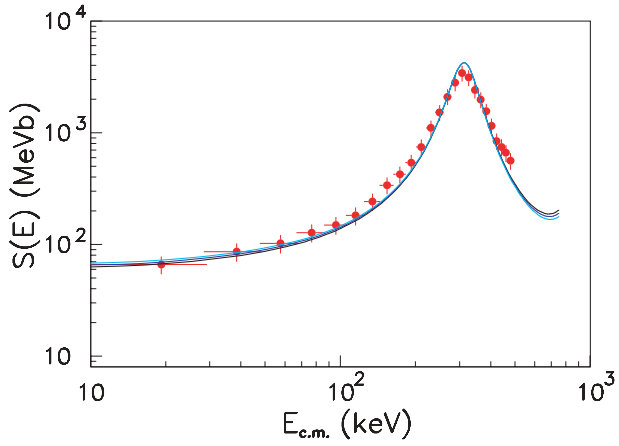

FIG. 11. (Color online) Comparison of the modified HOES R-matrix calculations of the $S^{\rm TH}(E_{xA}) \equiv S(E)$ astrophysical factor (full lines) with THM data (red dots), for a number of interaction radii: 4.5 fm (black), 5.0 fm (blue), and 5.5 fm (light blue). See text for details.

An estimate of the effect of the d-^{15}N scattering in the initial state on the energy dependence of the binary cross section can be obtained by taking into account only the Coulomb d-^{15}N interaction. We disregarded the n-^{16}O* interaction because the effect of the interaction of the spectator with the $^{15}\mathrm{N} + p$ system is significantly diminished in QF kinematics. To simplify calculations we assumed zero-range potential V_{Ax}. In this case if we take into account $d - {}^{15}$N Coulomb scattering in the initial state, the factor $|\varphi_a(p_{sx})|^2$ in Eq. (28) should be replaced by $|J|^2$, where

$$J(\mathbf{k}_s, \mathbf{k}_a) = \left\langle \varphi_a(\mathbf{k}_s - (m_s/m_a)\,\mathbf{k}'_a) \middle| \psi^{(C)(+)}_{\mathbf{k}_a}(\mathbf{k}'_a) \right\rangle. \quad (36)$$

Here the integration is performed over $\mathbf{k}'_a$ and $\psi^{(C)(+)}_{\mathbf{k}_a}(\mathbf{k}'_a)$ is the Fourier component of the $a - A$ Coulomb scattering wave function. Equation (36) is written in the center-of-mass of the TH reaction, so $\mathbf{k}_{aA} \equiv \mathbf{k}_a$ and $\mathbf{k}_{sF} \equiv \mathbf{k}_s$. We find that including Coulomb scattering in the initial state changes the energy dependence of the binary cross section in the energy interval $0 \leqslant E_{Ax} \leqslant 320$ keV by 3.5%. Because we are interested only in the behavior of the binary $^{15}\mathrm{N}(p,\alpha)^{12}\mathrm{C}$ reaction cross section as a function of energy, we use the plane-wave approximation in the initial and final states below. Note that the plane wave in the final state describes the relative motion of the neutron and the center-of-mass of the system $F = {}^{15}\mathrm{N} + p = {}^{12}\mathrm{C} + \alpha$.

VII. CONCLUSIONS

In the present article we have reported on an improved determination of the astrophysical S factor for the $^{15}\mathrm{N}(p,\alpha)^{12}\mathrm{C}$ reaction, as regards both previous indirect (THM) and direct measurements. Concerning the previous THM measurement, owing to a larger data sample (two couples of coincidence detectors) and an accurate investigation of all the sources of systematic uncertainties (including normalization to direct data and adopted theoretical framework in the S-factor extraction), both statistical and systematic errors are reduced with respect to the analysis discussed in Ref. [31]. Concerning direct data, the present knowledge of the $^{15}\mathrm{N}(p,\alpha)^{12}\mathrm{C}S(E)$ factor has been extended down to 20 keV (to be compared to 73 keV in direct measurements), thus covering for the first time the whole Gamow window (94 ± 66 keV for a temperature of 10^8 K). Moreover the $S(E)$ factor obtained via the THM is free of electron screening because the TH cross section is evaluated at energies much higher than the Coulomb barrier, thus this systematic uncertainty is not introduced in further astrophysical considerations. However, no electron screening potential has been deduced from the comparison with direct data owing to the experimental errors affecting both data sets, which are larger ($\sim$20%) than the expected enhancement of the S factor due to electron screening (about 10% at $\sim$70 keV). Indeed under these conditions the deduced U_e would be affected by a large systematic error that would make it worthless. Therefore more accurate low-energy measurements extending below about 70 keV are required to allow for the

extraction of U_e. The actual result confirms the Breit-Wigner extrapolation by Ref. [6], which is used to derive the reaction rate for astrophysical applications [4]. Here for the first time we took into account the Coulomb interaction between the colliding nuclei in the initial state of the TH reaction and off-energy-shell effects in the reaction. It was shown that the initial Coulomb scattering does not affect the extracted astrophysical factor. To take into account off-shell effects, we applied the HOES R-matrix approach. We have shown that the off-shell effects do not affect the energy dependence of the THM astrophysical factor for this system. The calculated astrophysical factor, within the framework of the HOES R-matrix approach, is in excellent agreement with direct data and THM results, as seen in Fig. 11. This justifies the application of the THM in extracting the low-energy S factor of astrophysically relevant resonant nuclear reactions.

The present results do not change the conclusions drawn from direct measurement but put them on more solid footing. Other relevant reaction rates which play an important role in determining ^{19}F abundance in AGB stars, such as ^{18}O$(p, \alpha)^{15}$N and ^{19}F$(\alpha, p)^{22}$Ne, are being studied with the same procedure.

ACKNOWLEDGMENTS

This work was supported by the U. S. Department of Energy under Grant No. DE-FG02-93ER40773.

[1] A. Renda *et al*., Mon. Not. R. Astron. Soc. **354**, 575 (2004).
[2] M. Lugaro *et al*., Astrophysical J. **615**, 934 (2004).
[3] A. Jorissen *et al*., Astronomy and Astrophysics **261**, 164 (1992).
[4] C. Angulo *et al*., Nucl. Phys. **A656**, 3 (1999).
[5] G. R. Coughlan and W. A Fowler, At. Data Nucl. Data Tables **40**, 283 (1988).
[6] A. Redder *et al*., Z. Phys. A **305**, 325 (1982).
[7] H. J. Assenbaum *et al*., Z. Phys. A **327**, 461 (1987).
[8] G. Fiorentini *et al*., Z. Phys. A **350**, 289 (1995).
[9] F. Strieder *et al*., Naturwissenschaften **88**, 461 (2001).
[10] M. La Cognata *et al*., Phys. Rev. C **72**, 065802 (2005).
[11] G. Baur *et al*., Nucl. Phys. **A458**, 188 (1986).
[12] G. Baur and H. Rebel, J. Phys. G **20**, 1 (1994).
[13] G. Baur and H. Rebel, Annu. Rev. Nucl. Part. Sci. **46**, 321 (1996).
[14] C. A. Bertulani and M. Gai, Nucl. Phys. **A636**, 227 (1998).
[15] T. Motobayashi, Eur. Phys. J. A **13**, 207 (2002).
[16] G. Baur *et al*., Prog. Part. Nucl. Phys. **51**, 487 (2003).
[17] H. M. Xu, C. A. Gagliardi, R. E. Tribble, A. M. Mukhamedzhanov, and N. K. Timofeyuk, Phys. Rev. Lett. **73**, 2027 (1994).
[18] A. M. Mukhamedzhanov *et al*., Phys. Rev. C **56**, 1302 (1997).
[19] A. Azhari *et al*., Phys. Rev. C **60**, 055803 (1999).
[20] C. A. Gagliardi *et al*., Phys. Rev. C **59**, 1149 (1999).
[21] A. M. Mukhamedzhanov and R. E. Tribble, Phys. Rev. C **59**, 3418 (1999).
[22] A. Azhari *et al*., Phys. Rev. C **63**, 055803 (2001).
[23] A. M. Mukhamedzhanov *et al*., Phys. Rev. C **63**, 024612 (2001).
[24] C. A. Gagliardi *et al*., Eur. Phys. J. A **13**, 227 (2002).
[25] X. D. Tang *et al*., Phys. Rev. C **67**, 015804 (2003).
[26] G. Baur, Phys. Lett. **B178**, 135 (1986).
[27] C. Spitaleri, *Problems of Fundamental Modern Physics II* (World Scientific, Singapore, 1990), pp. 21–35.
[28] S. Cherubini *et al*., Astrophysical J. **457**, 855 (1996).
[29] S. Typel and H. Wolter, Few-Body Syst. **29**, 7 (2000).
[30] S. Typel and G. Baur, Ann. Phys. **305**, 228 (2003).
[31] M. La Cognata *et al*., Eur. Phys. J. A **27**, 249 (2006).
[32] D. R. Tilley *et al*., Nucl. Phys. **A564**, 1 (1993).
[33] I. S. Shapiro, Proceedings of the XXXVIII International School of Physics "Enrico Fermi" (Academic Press, New York and London, 1967), p. 210.
[34] N. S. Chant and P. G. Roos, Phys. Rev. C **15**, 57 (1977).
[35] G. F. Chew, Phys. Rev. **80**, 196 (1950).
[36] G. Jacob and Th. A. Maris, Rev. Mod. Phys. **38**, 121 (1966).
[37] M. Jain *et al*., Nucl. Phys. **A153**, 49 (1970).
[38] A. Guichard *et al*., Phys. Rev. C **4**, 700 (1971).
[39] A. K. Jain *et al*., Nucl. Phys. **A216**, 519 (1973).
[40] D. Miljanić *et al*., Nucl. Phys. **A215**, 221 (1973).
[41] D. Miljanić *et al*., Phys. Lett. **B50**, 330 (1974).
[42] J. Kasagi *et al*., Nucl. Phys. **A239**, 233 (1975).
[43] V. G. Neudatchin and Y. F. Smirnov, Atom. Energ. Rev. **3**, 157 (1965).
[44] P. G. Roos *et al*., Phys. Rev. C **15**, 69 (1977).
[45] I. Slaus *et al*., Nucl. Phys. **A286**, 67 (1977).
[46] A. M. Mukhamedzhanov *et al*., Eur. Phys. J. A **27**, 205 (2006).
[47] C. Spitaleri *et al*., Phys. Rev. C **63**, 055806 (2004).
[48] M. Lattuada *et al*., Ap. J. **562**, 1076 (2001).
[49] A. Musumarra *et al*., Phys. Rev. C **64**, 068801 (2001).
[50] C. Spitaleri *et al*., Phys. Rev. C **63**, 005801 (2001).
[51] A. Tumino *et al*., Nucl. Phys. **A718**, 499 (2003).
[52] A. Tumino *et al*., Phys. Rev. C **67**, 065803 (2003).
[53] A. M. Mukhamedzhanov *et al*., arXiv:0708.0658[nucl-th] (2007).
[54] C. Mahaux and H. A. Weidenmüller, *Shell-Model Approach to Nuclear Reactions* (North-Holland, Amsterdam, 1969).
[55] A. M. Lane and R. G. Thomas, Rev. Mod. Phys. **30**, 257 (1958).
[56] H. Fuchs *et al*., Phys. Lett. **B37**, 285 (1971).
[57] A. M. Mukhamedzhanov *et al*., Nucl. Phys. **A787**, 321 (2007).
[58] A. Schardt *et al*., Phys. Rev. **86**, 527 (1952).
[59] J. L. Zyskind *et al*., Nucl. Phys. **A320**, 404 (1979).
[60] C. Rolfs and W. S. Rodney, Nucl. Phys. **A235**, 450 (1974).
[61] F. Ajzenberg-Selove, Nucl. Phys. **A523**, 1 (1991).
[62] C. Spitaleri *et al*., Phys. Rev. C **60**, 055802 (1999).
[63] C. Spitaleri *et al*., Eur. Phys. J. A **7**, 181 (2000).
[64] M. Aliotta *et al*., Eur. Phys. J. A **9**, 435 (2000).
[65] G. Calvi *et al*., Nucl. Phys. **A621**, 139c (1997).
[66] M. La Cognata *et al*., Nucl. Phys. **A758**, 98 (2005).
[67] L. Lamia *et al*., Nucl. Phys. **A787**, 307c (2007).
[68] M. G. Pellegriti *et al*., Nucl. Phys. **A688**, 543 (2001).
[69] M. G. Pellegriti *et al*., Prog. Theor. Phys. Suppl. **154**, 349 (2004).
[70] R. G. Pizzone *et al*., Nucl. Phys. **B118**, 455 (2003).
[71] R. G. Pizzone *et al*., Nucl. Phys. **A718**, 496 (2003).
[72] A. Rinollo *et al*., Nucl. Phys. **A758**, 146 (2005).
[73] S. Romano *et al*., Nucl. Phys. **A738**, 406 (2004).
[74] S. Romano *et al*., Eur. Phys. J. A **27**, 221 (2006).
[75] A. Tumino *et al*., Prog. Theor. Phys. Suppl. **154**, 341 (2004).
[76] A. Tumino *et al*., Eur. Phys. J. A **25**, 649 (2005).
[77] A. Tumino *et al*., Eur. Phys. J. A **27**, 243 (2006).